TRENDS IN LIFETIME MEASUREMENTS

Dieter K. Schroder
Department of Electrical Engineering
Center for Solid State Electronics Research
Arizona State University
Tempe, AZ 5287-5706

Abstract

The interpretation of lifetime measurements and new characterization techniques are addressed in this paper. Parameters such as surface/interface recombination, sample thickness, and injection level are discussed. Novel characterization techniques using frequency-dependent capacitance, conductance, or impedance measurements are described and are shown to be useful for thin layer, e.g., epitaxial or silicon-on-insulator layers, characterization.

Introduction

Lifetime was one of the earliest parameters to be measured during the evolution of semiconductors. For example, one the parameters determined in the classic Haynes-Shockley experiment during the early 1950s, is the minority carrier lifetime.[1] After the initial flurry of developing numerous lifetime characterization techniques, the topic lost some of its appeal and went into a decline for many years. Of course, people made lifetime measurements, but the equipment was frequently home made, samples had to carefully prepared, and the interpretation was not always unambiguous.

It was only when commercial equipment became available, that significant progress was made. Measurements made by Si wafer producers and integrated circuit (IC) companies generated a wealth of data, usually displayed as color maps for any size wafer. These measurements were generally made contactless with all necessary data processing built into the equipment. The silicon crystal growers measured lifetimes to characterize the Czochralski crystal pullers and the growth process and the IC companies used these measurements to follow the cleanliness of their processes.

A major impact on lifetime measurements, was the discovery of iron-boron pair formation and dissociation in 1981.[2] Initially, this was merely an interesting phenomenon, but was not exploited. It was only when Zoth and Bergholz pointed out that by measuring the minority carrier lifetime or the recombination lifetime during the Fe-B state and then during the interstitial iron, Fe_i, state in boron-doped wafers, was it possible to determine the iron density in a wafer.[3] Since iron is also one of the chief metallic impurities introduced during wafer processing, iron being one the main constituents of the ubiquitous stainless steel, this was an ideal combination of simple, contactless diffusion length/lifetime measurements with iron detection in commercial equipment. It spawned several new characterization tools.

Now that lifetime measurements are routinely made, attention has shifted from the basic measurements to interpretation of the measured data in today's Si wafer/process technology and development of novel lifetime characterization techniques. Such parameters as injection level, temperature, frequency dependence and others are being actively looked at for lifetime data interpretation. I will focus on several aspects of lifetime characterization and interpretation and will assume the reader to be familiar with the concept of lifetimes and the basic measurement techniques. Epitaxial layer characterization

through conventional recombination lifetime measurements is difficult, because the epi layers are typically much thinner than the minority carrier diffusion length, making the data analysis difficult. This difficulty also applies to today's bulk Si wafers. They are so pure that they have exceedingly high lifetimes. This makes surface recombination much more important than in the past.

The bulk recombination lifetime τ_B in its simplest form is given by

$$\tau_B = \frac{1}{\sigma_n v_{th} N_T} \tag{1}$$

where σ_n is the minority carrier capture cross section, v_{th} the thermal velocity, and N_T the defect density. For $\sigma_n = 10^{-14}$ cm^2 and $v_{th} = 10^7$ cm/s, τ_B becomes

$$\tau_B = \frac{10^7}{N_T} \tag{2}$$

High-quality Si wafers contain defect densities on the order of 10^{10} cm^{-3}, leading to $\tau_B \approx 10^{-3}$ s. The minority carrier diffusion length, given by $L_n = (D_n \tau_B)^{1/2}$, for such high lifetime material is about 2000 μm - much longer than typical wafer thicknesses of 500-850 μm. Such long diffusion lengths make the correct determination of L_n or τ_r very difficult, because the theory that is usually used to analyze the data is based on simplifying assumptions of the more detailed, complete equations.

Surfaces characterized through their surface recombination velocities become more important as bulk lifetimes increase. The effective recombination lifetime τ_{reff} due to bulk lifetime τ_B and surface lifetime τ_s is given by

$$\tau_{reff} = \frac{\tau_B \tau_s}{\tau_B + \tau_s} \tag{3}$$

The surface lifetime due to surface or interface recombination is

$$\tau_s = \frac{t}{2\sigma_n v_{th} N_s} = \frac{t}{2s_r} \tag{4}$$

where t is the sample thickness, N_s the surface or interface state density, and s_r the surface recombination velocity. For t = 750 μm, $\sigma_n = 10^{-15}$ cm^2, and $v_{th} = 10^7$ cm/s, the surface lifetime becomes

$$\tau_s = \frac{3.75x10^6}{N_s} \tag{5}$$

Bare Si surfaces have surface state densities on the order of 10^{12} cm^{-2}, leading to $\tau_s \approx 4x10^{-6}$ s. Oxidized and well annealed Si surfaces have interface state densities of around 10^{10} cm^{-2}, giving $\tau_s \approx 4x10^{-4}$ s. Either one of these values is lower than the 10^{-2} s bulk lifetime, making surface recombination the dominant mechanism. It is only when N_s approaches 10^8 cm^{-2} ($\tau_s \approx 4x10^{-2}$ s) that τ_s approaches τ_B. This situation is further aggravated if the sample becomes thinner, *e.g.*, epitaxial layers. The epitaxial layer thickness is

typically several microns for most IC applications. According to Eq. (3), this reduces the surface lifetime even further. So we have arrived at the ironic situation where lifetime measurements have become easy and routine, but their interpretation is increasingly difficult.

The effect of surface recombination is illustrated in Fig. 1, showing the effective recombination lifetime as a function of iron density for iron in both its Fe-B and Fe_i states. τ_{reff} saturates at low iron densities due to surface recombination. As metal densities decrease further, it is obvious from Fig. 1 that extraction of bulk impurity densities becomes increasingly difficult due to surface recombination.

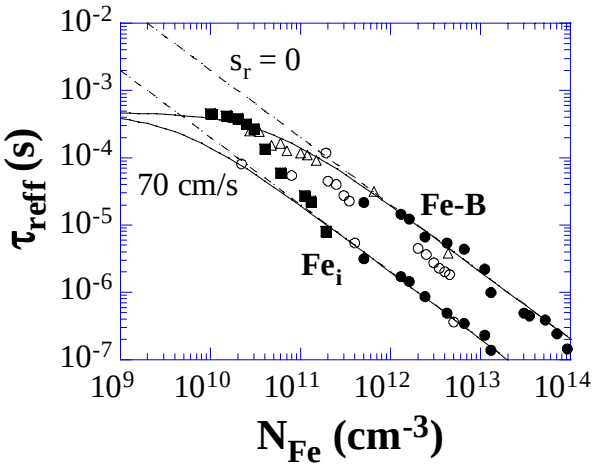

Fig. 1 Effective recombination lifetime versus iron density. The points are experimental data and the lines are calculated for two different surface recombination velocities. Data are taken from ref. 4.

Considering the epi layer lifetime as τ_{epi}, the surface lifetime as τ_{s1} and the epi/substrate interface lifetime as τ_{s2} the net effective lifetime is[4]

$$\frac{1}{\tau_{reff}} = \frac{1}{\tau_{epi}} + \frac{1}{\tau_{s1}} + \frac{1}{\tau_{s2}} \approx \frac{1}{\tau_{epi}} + \frac{2s_{r1}}{t_{epi}} + \frac{2s_{r2}}{t_{epi}} \qquad (6)$$

where t_{epi} is the epitaxial layer thickness and s_r the surface or interface recombination velocity. To illustrate the effect of surface/interface recombination on the recombination properties, we have plotted τ_{reff} versus epi layer thickness as a function of epi layer lifetime in Fig. 2, for $s_{r1} = s_{r2} = 1$ cm/s and 100 cm/s. For $t_{epi} < 4s_r\tau_{epi}$, the effective lifetime is dominated by interfacial recombination and for $t_{epi} > 4s_r\tau_{epi}$ by epitaxial layer recombination. For typical epi layer thicknesses of 10^{-4} to 10^{-3} cm, the effective lifetime is largely dominated by interfacial recombination for lifetimes of 100 μs or higher. The lifetime of high quality bulk Si wafers is typically in the 1-10 ms range while that in epi layers is on the order of 100 μs. Epi layer lifetimes are typically lower than those of bulk wafers, because their metallic contamination density is higher.

The surface recombination velocity can be altered substantially through external means. For example, while a bare Si surface may have $s_r \approx 10^4$ cm/s or higher, oxidized surfaces have $s_r \approx$ 10-100 cm/s. Immersing the sample in dilute HF or iodine/methanol solutions can bring the surface recombination velocity to 1-10 cm/s. Depositing corona charge allows the wafer surface to be brought into accumulation with a resulting very low s_r of 1 cm/s or less.[5] Fig. 2 shows that for sufficiently low surface recombination velocities, it is possible for lifetime measurements to provide some information about the epi

layer, even though the effective lifetime is only vaguely related to the true lifetime. By taking differences, it is possible to determine the iron contamination in epitaxial layers.[6]

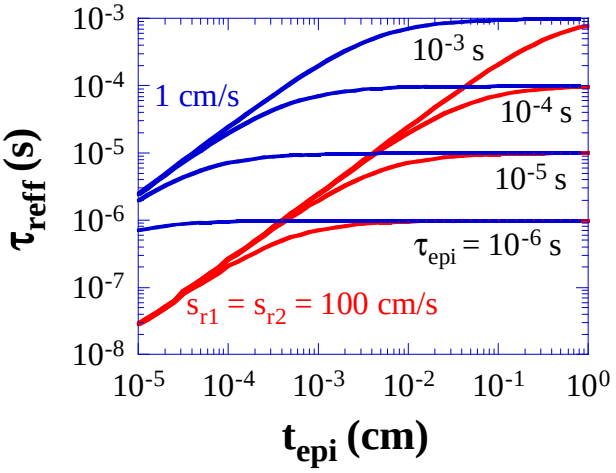

Fig. 2 Effective recombination lifetime versus epitaxial layer thickness as a function of epi layer lifetime and surface recombination velocity.

Surface photovoltage measurements with penetrating light have the problem that ehps are generated in both the epi layer and the substrate, but the minority carrier diffusion length L_n in the heavily-doped substrate is usually much lower than that in the epi layer. Hence, the measurements typically yield t_{epi} rather than L_n.

Due to these difficulties, space-charge region measurements are usually made with electron-hole pair generation/recombination largely confined to the scr. Such methods include measurements of the leakage current of reverse-biased pn junctions,[7] the recovery time of pulsed MOS capacitors,[8] or the frequency dependence of scr-dependent parameters.[9] The emergence of commercially available, corona-based semiconductor characterization tools has opened up the possibility of making such lifetime measurements on oxidized Si wafers without having to fabricate devices.[10] The reverse-biased junction current density is given by

$$J = \frac{qn_i W}{\tau_g} + \frac{qn_i^2 D_n}{N_{A,epi} L_n} \tag{7}$$

where q is the electron charge, W the scr width, n_i the intrinsic carrier density, τ_g the generation lifetime, D_n the diffusion coefficient, and $N_{A,epi}$ the epi layer doping density. It is important during these measurements to ascertain that scr generation dominates. Quasi-neutral region (qnr) generation, usually negligible at room temperature, becomes important at elevated temperatures.

For epitaxial layers, one should correctly use an effective diffusion length L_{neff} given by

$$L_{neff} = \frac{L_n}{F} \tag{8}$$

with the correction factor F given by[11]

$$F = \frac{(1 + N_{A,sub}/N_{A,epi})\exp(t/L_n) + (1 - N_{A,sub}/N_{A,epi})\exp(-t/L_n)}{(1 + N_{A,sub}/N_{A,epi})\exp(t/L_n) - (1 - N_{A,sub}/N_{A,epi})\exp(-t/L_n)} \tag{9}$$

where t is the undepleted epi layer thickness and $N_{A,sub}$ the substrate doping density. Clearly for long diffusion length and high $N_{A,sub}$, the correction factor becomes substantial making L_{neff} significantly higher than L_n. In spite of the diffusion length uncertainty, scr measurements are effective epi layer characterization techniques.

Space-charge region based measurements can be augmented with optical excitation and contactless Kelvin probe detection. We present in this paper the relevant theory, supported by experimental data, of charge-based, light-excited Kelvin probe measurements of epitaxial layers. We show that for short wavelength light, with optically generated carriers largely confined to the space-charge region, we do, in fact characterize the epitaxial layer, by measuring the recombination lifetime in the space-charge region.

Injection Level Dependent Lifetimes

Lifetimes in silicon are governed by Shockley-Read-Hall (SRH) recombination for doping densities of 10^{17} cm^{-3} or less. The SRH lifetime is given by[12]

$$\tau_{SRH} = \frac{\tau_p(n_o + n_1 + \Delta n) + \tau_n(p_o + p_1 + \Delta p)}{p_o + n_o + \Delta n} \tag{10}$$

where $\tau_p = 1/\sigma_p v_{th} N_T$, $\tau_n = 1/\sigma_n v_{th} N_T$, $n_1 = n_i \exp[(E_T - E_i)/kT]$, $p_1 = n_i \exp[-(E_T - E_i)/kT]$, and Δn and Δp are the excess carrier densities. For low-level injection, the excess carrier density is much lower than the equilibrium majority carrier density and for high-level injection it is much higher. Generally, photoconductance decay (PCD) measurements are made under high-level injection and surface photovoltage (SPV) measurements are made under low-level injection. Occasionally, lifetimes are measured as a function of injection level. Such measurements contain additional information. The ELYMAT technique[13] lends itself very well for this, as does PCD. Such measurements provide additional information.

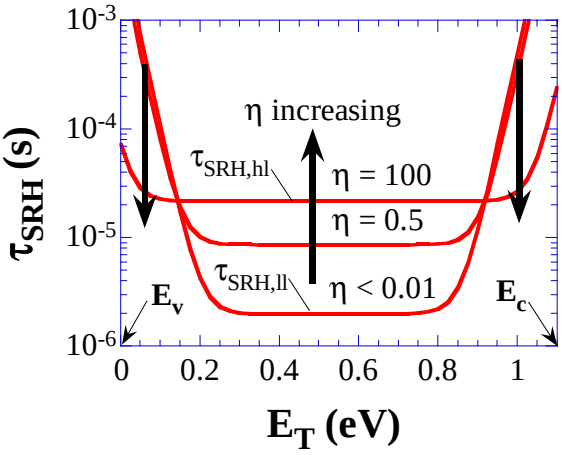

Fig. 3 τ_{SRH} versus E_T as a function of injection level, $\eta = \Delta n/p_o$, for $N_T = 10^{12}$ cm^{-3}, $p_o = 10^{16}$ cm^{-3}, $\sigma_n = 5\text{x}10^{-14}$ cm^2, and $\sigma_p = 5\text{x}10^{-15}$ cm^2. p_o is the equilibrium majority carrier density.

Plotting τ_{SRH} from Eq. (10) versus the impurity energy level E_T as a function of injection level gives the curves in Fig. 3. Although it is frequently assumed that the lifetime increases with injection level, for impurities with energy levels near the conduction or valence bands, the opposite is true as indicated by the arrows in Fig. 3. Since most impurities have energy levels towards the central portion of the band gap, the lifetime does generally increase with injection level. However, Fe-B pairs, with an energy level of about 0.1 eV above the valence band, clearly fall in the category of shallow-level impuri-

ties with decreasing lifetime with increasing injection level.

Experimental lifetime data for several impurities in Si are shown in Fig. 4. The lifetime of Fe-B pairs does indeed decrease with injection level while that of interstitial iron increases. The lifetime due to Cr increases slightly, while the lifetime due to oxygen precipitates is very injection level dependent, varying in this example by almost three orders of magnitude. These examples illustrate that the injection level provides an additional variable that can be very useful in identifying the nature of certain impurities. Injection level is typically varied by changing the bias conditions on the laser that is used for optical excitation in PCD[14] and ELYMAT[13] measurements or with neutral density filters. Surface photovoltage measurements are rarely made at high level injection. Very high light intensity SPV measurements are used to determine surface charges by flattening the bands.[15]

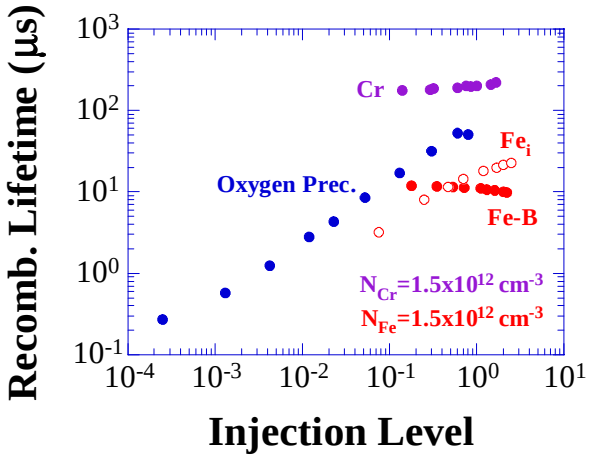

Fig. 4 τ_{SRH} versus injection level. Data after Eichinger (ref. 13).

Frequency-dependent Lifetime Characterization

Most carrier lifetime or minority carrier diffusion length measurements are made in the time domain (photoconductance decay and pulsed MOS capacitor measurements), or in steady state (surface photovoltage and diode leakage current measurements). The theory and interpretation of such measurements is well in hand. The advent of some recently introduced lifetime characterization equipment allows lifetime measurements to be made in the frequency domain. This offers some advantages over conventional measurements, but the theory is not as well developed. It is, of course, well known that frequency-domain measurements contain similar information as time-domain measurements. We present the theory, complemented by experimental data, of two different approaches to frequency-domain measurements. In one approach, the device is a gate-controlled device, *e.g.*, MOS capacitor or Kelvin probe, with *frequency-dependent electrical excitation*. In the other, a surface charge-induced space-charge region is created and the device is excited with low-level, *frequency-modulated light*. The lifetime or diffusion length is extracted from the resultant frequency-dependent capacitance, conductance, or impedance.

Electrical Excitation

The equivalent circuit concept to describe and analyze semiconductor devices has proven to be very powerful. Some of the earliest papers dealing with the equivalent circuit of the MOS capacitor are due to Lehovec and Slobodskoy[16] and Hofstein and

Warfield.[17] A detailed discussion of equivalent circuits for MOS capacitors can be found in the Nicollian/Brews book.[18] We present the theory of frequency-domain measurements, by considering MOS capacitors (MOS-C). Such devices are appropriate because recent implementations of measurement techniques use Kelvin probes and/or corona charge as the "gate" electrode. Such implementations can be viewed as a form of MOS capacitor. A MOS-C is best suited for lifetime characterization when biased in inversion, because then we are concerned with the generation and recombination of minority carriers in the inversion layer. That is not the case in depletion or accumulation, where only majority carriers are important.

Theory

The equivalent circuit in Fig. 5(a) represents the MOS-C on a *p*-type substrate. It consists of the gate oxide capacitance (C_{ox}), the inversion charge capacitance (C_N), the accumulation charge capacitance (C_P), the interface trapped charge capacitance (C_{it}), and the space-charge region capacitance (C_B) as well as their corresponding conductances and the series resistance R_s and C_s the substrate capacitance. The R_sC_s time constant or the dielectric relaxation time, is important only when the lifetime is on the order of the relaxation time. This is only relevant for high resistivity material as used for Si radiation detectors, for example.

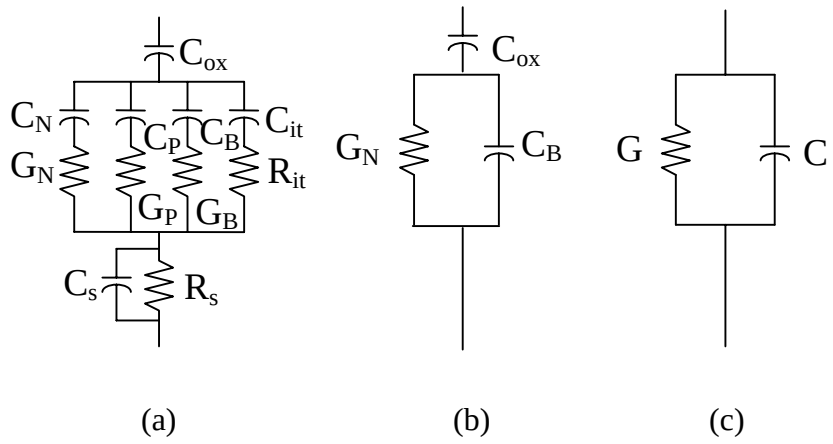

Fig. 5 (a) Equivalent circuit, (b) reduced equivalent circuit, (c) measured circuit

In inversion, the hole density near the surface for a p-type substrate is very low, making the majority carrier capacitance C_P small, allowing it to be treated as an open circuit. By the same token, the surface electron density is very high, making the inversion charge capacitance C_N high, allowing it to be replaced by a short circuit. The interface state density of oxidized and annealed Si samples is low, allowing the interface state capacitance to be neglected. The bulk conductance G_B of the space-charge capacitance is high due to the fast majority carrier response and we will replace it by a short circuit. Further, we will neglect the series resistance R_s. This allows the equivalent circuit to be simplified to that in Fig. 5(b). We will, furthermore, neglect interface trap effects.

Simplifying the circuit further to one actually determined by measurement gives Fig. 5(c) with an admittance of

$$Y = G + jB = G + j\omega C \tag{11}$$

where G is the conductance and B the susceptance. Through a straightforward but tedious circuit conversion, we find for the equivalent capacitance and conductance the following expressions

$$C = \frac{1+(\omega/\omega_2)(\omega/\omega_1+\omega/\omega_2)}{1+(\omega/\omega_1+\omega/\omega_2)^2}C_{ox};\ G = \frac{(\omega/\omega_1)}{1+(\omega/\omega_1+\omega/\omega_2)^2}\omega C_{ox} \tag{12}$$

where ω is the radial frequency $\omega = 2\pi f$ (f is the frequency) and

$$\omega_1 = \frac{G_N}{C_{ox}};\ \omega_2 = \frac{G_N}{C_B} \tag{13}$$

These expressions are identical to those of Baccarani et al. if in their expression we let the inversion capacitance become very high.[19]

The *space-charge region* generation rate G_{scr} and conductance $G_{N,scr}$ are[9]

$$G_{scr} = I_{scr} = \frac{qAn_iW}{\tau_g};\ G_{N,scr} = \frac{I_{scr}}{V} = \frac{qAn_iW}{\tau_g\phi_s} = \frac{2K_s\varepsilon_o An_i}{\tau_g N_A W} \tag{14}$$

where W is the scr width, τ_g the generation lifetime, A the area, and ϕ_s the surface potential, *i.e.*, the voltage across the semiconductor substrate. We take the surface potential in inversion as $\phi_s = qN_AW^2/2K_s\varepsilon_o = 2\phi_F$, *i.e.*, twice the Fermi potential. ϕ_s is actually a few kT/q higher than $2\phi_F$, but this is a minor effect, that we neglect. T is the temperature, N_A is the wafer doping density and n_i the intrinsic carrier density.

The *quasi-neutral region* generation rate G_{qnr} and conductance $G_{N,qnr}$ are[9]

$$G_{qnr} = I_{qnr} = \frac{qAn_i^2D_n}{N_AL_n};\ G_{N,qnr} = \frac{I_{qnr}}{V} = \frac{qAn_i^2D_n/N_AL_n}{kT/q} = \frac{qA\mu_n n_i^2}{N_AL_n} \tag{15}$$

where D_n is the electron diffusion constant and μ_n the electron mobility. We have used the voltage drop across the qnr region as kT/q, appropriate for the voltage drop due to minority carrier diffusion. For the diffusion length, we simply use L_n so the wafer must be at least 3-4 diffusion lengths thick. If that is not the case, then we need to use the modified diffusion length. Our approximation, however, does not affect the theory developed here.

The frequency-dependent recombination and generation lifetimes are taken to be $\tau_r = \tau_{ro}/(1+j\omega\tau_{ro})$ and $\tau_g = \tau_{go}/(1+j\omega\tau_{go})$ in our analysis. This modification from the standard lifetimes of τ_r and τ_g is due to the ac signal excitation and can be derived from the ac continuity equation. For simplicity, we have taken τ_{go} as constant with temperature, although it is approximately given by $\tau_{go} \approx \tau_{ro}\exp[(E_T-E_i)/kT]$. Our results indicate that neither the capacitance nor the conductance is sensitive to the generation lifetime for the conditions we use.

To see the behavior of scr and qnr generation, we plot in Fig. 6 the capacitance and conductance calculated with Eq. (12). To determine the lifetime, we need to know the break frequencies ω_1 or ω_2. ω_1 cannot be readily determined from either capacitance or conductance. However, ω_2 can be obtained from the capacitance as the lower break-

point. The mid frequency $\omega_{mid} = \omega_1\omega_2/(\omega_1+\omega_2)$, readily determined as the midpoint on the capacitance and the breakpoint on the conductance curves, is

$$\omega_{mid} = \frac{G_N}{C_{ox}+C_B} = \frac{2n_i/\tau_g + q\mu_n n_i^2 W/K_s\varepsilon_o L_n}{N_A(1+K_{ox}W/K_s t_{ox})} \tag{16}$$

The inverse lifetime τ_{ro} is easiest determined from the second breakpoint on the G - ω curve. It is obvious from Eq. (16) that neither τ_g nor L_n is easily extracted from ω_{mid}, unless one knows which of the two terms in the numerator dominates.

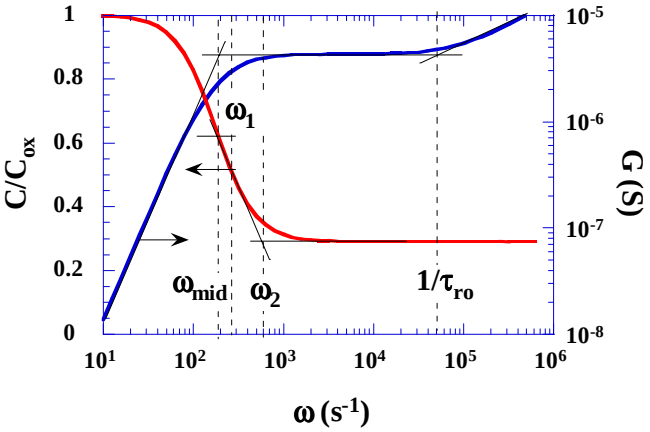

Fig. 6 Capacitance and conductance as a function of frequency.
τ_{ro} = 20 μs, τ_{go} = 1 ms, N_A = 10^{15} cm^{-3}, t_{ox} = 100 nm, T = 370 K, A = 1 cm^2.

In order to extract lifetime/diffusion length, the dependence of C and G depend on various material/device parameters must be known. One parameter frequently varied during the measurements is temperature. Here we must be very careful to point out what is measured. During diode leakage current and pulsed MOS capacitor lifetime measurements, one measures in effect the *generation rate*, G, because both capacitance transient decay and diode leakage current depend directly on the generation rate.

During frequency-dependent measurements, we measure the conductance or the capacitance. How do scr and qnr *conductances* behave as a function of temperature? As illustrated in Fig. 7, the breakpoint between scr and qnr domination occurs at T=285 K. Hence, measurements that rely on conductance or capacitance measurements as a function of frequency and confine their measurements to room temperature or above, find the device behavior *dominated by qnr generation*.

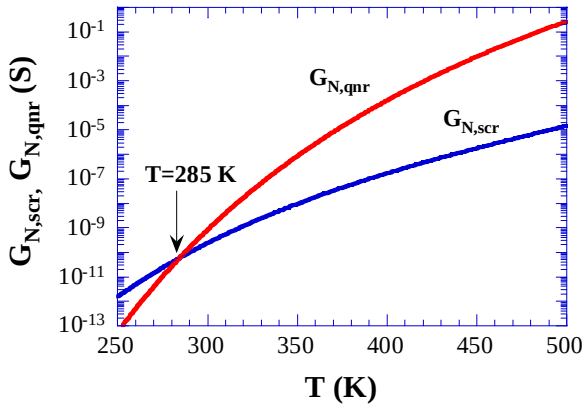

Fig. 7 Space-charge region and quasi-neutral region conductances versus temperature.
τ_{ro} = 20 μs, τ_{go} = 1 ms, N_A = 10^{15} cm^{-3}, A = 1 cm^2.

One might ask, so what? Well, if, for example one wants to determine the lifetime of a thin epitaxial layer, it is possible to do that through a measurement dominated by scr generation, since the generation width in that case is the scr width. If the measurement is dominated by qnr generation, then the appropriate width that is characterized is the minority carrier diffusion length L_n. But L_n is usually much longer than the epi layer thickness and diffusion length determination is poorly suited to characterize such layers. For generation rate measurements, it is reasonable to assume that room temperature characterization, in fact, determines τ_g. We see from Fig. 7, however, that conductance measurements are dominated by qnr generation even at room temperature and hence are characterized by τ_r or L_n, *not* by τ_g.

Experimental Results

We have measured several MOS capacitors and compared the measured data to theory. Fig. 8 gives the data for an iron-doped sample. Note the excellent agreement between theory and experiment for both the capacitance and the conductance data. We find the theoretical data to be independent of the generation lifetime for $\tau_g \geq 10^{-6}$ s, because both C and G are determined by qnr generation with scr generation being negligible.

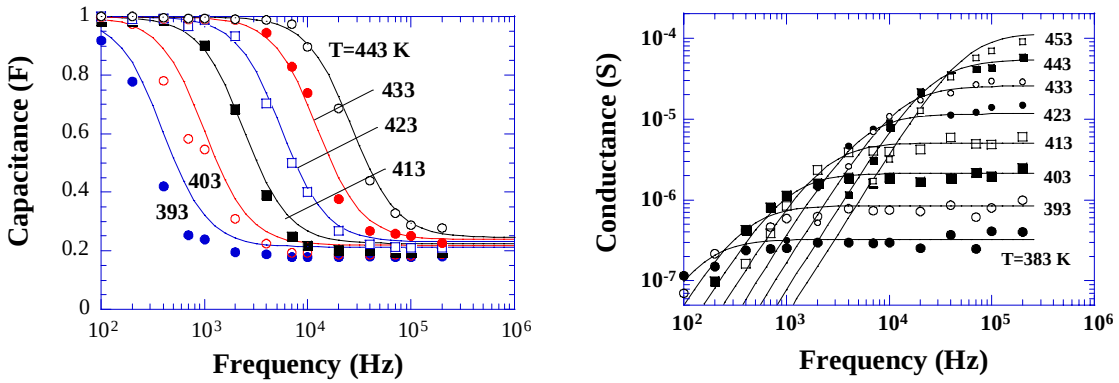

Fig. 8 Experimental (points) and calculated (lines) for Fe-doped Si.
τ_{ro} = 1.3 μs, τ_{go} = 100 μs, $N_A = 1.25 \times 10^{15}$ cm^{-3}, t_{ox} = 40 nm.

Optical Excitation

During corona-based measurements, corona charge is deposited on the wafer and its electrical response is measured by one of several techniques. One can drive the corona-oxide-semiconductor (COS) device into deep depletion and measure the recovery response with a contactless Kelvin probe.[10] It is also possible to bias the COS device into inversion and measure the frequency response by varying the electrical signal applied to the Kelvin probe or by applying a time-varying optical signal to the device.[20]

To understand corona charge-based measurements, it is necessary to understand Kelvin probe measurements. Lord Kelvin first proposed the Kelvin probe in 1881.[21] Kronik and Shapira give an excellent explanation of Kelvin probes and their various applications.[22] We will explain its operation with the aid of Fig. 9. Consider a *p*-type semiconductor with a grounded substrate. A metal probe, the Kelvin probe, is placed a distance d (typically 0.1 – 1 mm) from the wafer surface. In this discussion we assume the work functions of the metal and the semiconductor to be identical. With no surface charge on the semiconductor surface, the semiconductor bands are flat, as shown by the

dashed energy band diagram in Fig. 9(a) and the probe potential, also known as the contact potential difference V_{cpd}, is zero.

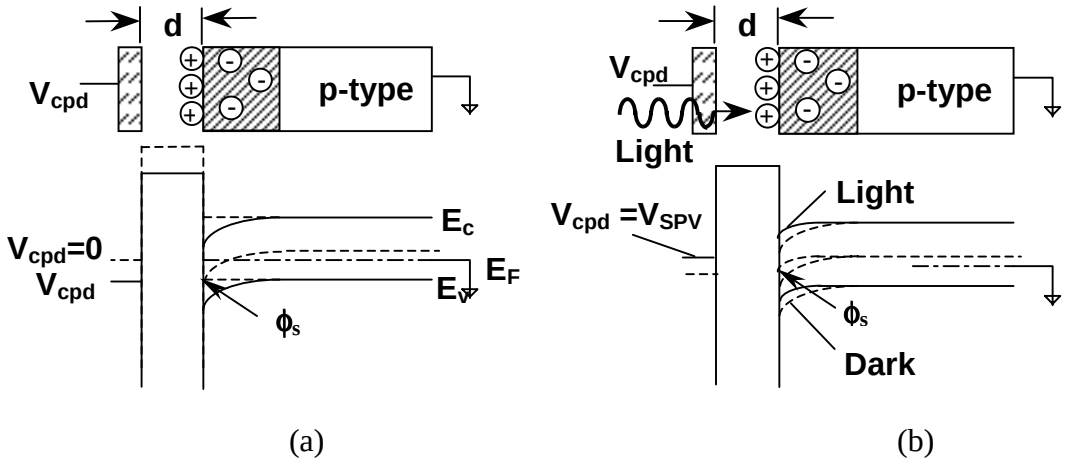

Fig. 9 The equivalent circuit of the SPV measurement system.

For positive surface charge, the semiconductor is depleted, as shown by the solid energy band diagram in Fig. 9(a). The electrically floating Kelvin probe will assume a positive contact potential difference V_{cpd} equal to the surface potential ϕ_s, since no charge can be deposited on the electrically floating probe and hence there is no electric field between the semiconductor surface and the probe. When the semiconductor is illuminated, the Fermi level splits into two quasi-Fermi levels and both the semiconductor band bending and V_{cpd} are reduced, as illustrated in Fig. 9(b). Since we are dealing with optically induced voltages in this paper, we will designate the probe voltage as the surface photovoltage V_{SPV}.

A crucial component for SPV measurements is the surface treatment to create the surface space-charge region. For *n*-type silicon, the oxide on the sample surface should be removed and then the sample should be boiled in H_2O_2 or in water for about 15 min and then rinsed in deionized water (DI).[23] Alternately, one can soak the sample in $KMnO_4$ for 1-2 min and then rinse in DI water. These treatments produce a stable depletion surface potential barrier. For *p*-type silicon very little treatment is required. In case of very low V_{SPV}, etching in buffered HF followed by a DI water rinse is recommended.

The energy band diagram of the probe-air-semiconductor system is analogous to that of a MOS capacitor with the insulator replaced with air. Positive charges deposited on the semiconductor surface deplete the surface of the p-type sample. Photons, incident on the sample, generate excess carriers within the space-charge region and in the quasi-neutral bulk region. The electrons within the scr and within a distance of approximately the minority carrier diffusion length from the edge of the scr will be collected in the space-charge region and reduce the surface potential barrier slightly. The barrier lowering is similar to a forward-biased junction and the Kelvin probe detects the difference of the quasi-Fermi levels. For high-level injection, the surface potential vanishes.[15] However, we use low-level injection leading to low surface potentials.

Theory

Charge on the surface of the *p*-type wafer induces a space charge of width *W*. Incident light generates electron-hole pairs (ehp) in the sample and the resulting surface

photovoltage is measured. The location of carrier generation depends on the wavelength of the incident light. We treat the general case of generation in both the space-charge region and in the quasi-neutral region. In general there is recombination of the excess carriers and generation. The equivalent circuit of Fig. 10 represents the semiconductor under ac light excitation. The monochromatic, ac-modulated light generates the photocurrent I_{ph}. The capacitance C_{scr} represents the surface charge-induced space-charge region. The conductances G represent the various loss mechanisms in the semiconductor. The losses occur when carriers recombine or are generated. Excess carriers at the surface recombine through surface states with a surface recombination velocity s_r, shown by conductance G_s. Thermal generation in the space-charge region as well as in the quasi-neutral bulk region is shown by $G_{g,scr}$ and $G_{g,qnr}$ and recombination in the scr and qnr regions as $G_{r,scr}$ and $G_{r,qnr}$.

We define conductances as current density divided by voltage in units of S/cm^2. The surface conductance G_s due to surface recombination is given by[9]

$$G_s = \frac{J_s}{V} \approx \frac{qD_n d(\delta n)/dx}{V_{SPV}} = \frac{qs_r \delta n}{V_{SPV}} = \frac{qs_r n_{po}[\exp(qV_{SPV}/kT)-1]}{V_{SPV}} \approx \frac{q^2 s_r n_{po}}{kT} = \frac{q^2 s_r n_i^2}{kTN_{A,epi}} \quad (17)$$

for low surface photovoltage, *i.e.*, $V_{SPV} < kT/q$. δn is the excess minority carrier density. The conductance G_g consists of the conductance $G_{g,scr}$ due to thermal generation in the space-charge region and $G_{g,qnr}$ due to thermal generation in the quasi-neutral region (qnr). It is given by[9]

$$G_g = G_{g,scr} + G_{g,qnr} = \frac{qK_s \varepsilon_o n_i}{\tau_g N_{A,epi} W} + \frac{q\mu_n n_i^2}{N_{A,epi} L_n} \quad (18)$$

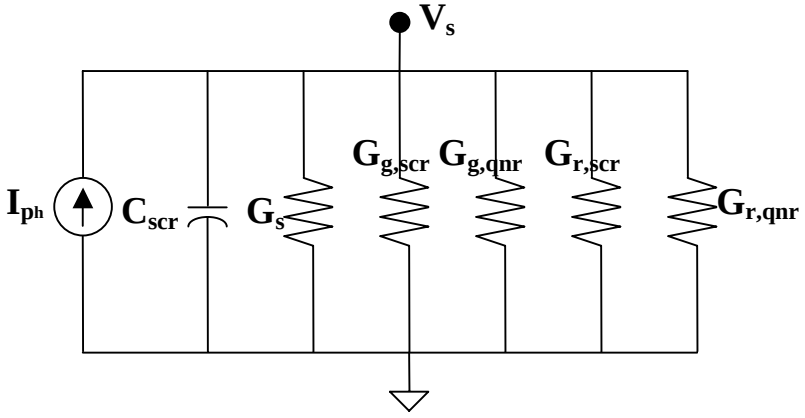

Fig. 10 The equivalent circuit of the SPV measurement system.

Optical carrier generation and carrier injection over a slightly forward-biased barrier leads to recombination in the space-charge region and to the conductance $G_{r,scr}$

$$G_{r,scr} = \frac{J_{r,scr}}{V_{SPV}} \approx \frac{\frac{qn_i W}{\tau_{scr}}(\exp(\frac{qV_{SPV}}{kT})-1)}{V_{SPV}} \approx \frac{q^2 n_i W}{\tau_{scr} kT} \quad (19)$$

which depends on n_i, W, and the scr recombination lifetime, τ_{scr}. In addition to these loss elements, there will be a qnr recombination conductance ($G_{r,qnr}$) due recombination in the quasi-neutral region given by

$$G_{r,qnr} = \frac{J_{r,qnr}}{V_{SPV}} \approx \frac{\frac{qn_i^2 D_n}{N_A L_n}(\exp(\frac{qV_{SPV}}{kT}) - 1)}{V_{SPV}} \approx \frac{q^2 n_i^2 D_n}{N_{A,epi} L_n kT} = \frac{q\mu_n n_i^2}{N_{A,epi} L_n} \tag{20}$$

The conductances for qnr recombination and generation are identical. This is expected for low voltages and is equivalent to the current of a pn junction being identical, except for a sign change, in both forward and reverse bias for diode voltages less than kT/q.

So far we have been concerned with dc behavior. Since we are ultimately interested in ac excitation, we need to consider the ac behavior of the various lifetimes. Mathematical analyses of steady-state solutions usually assume all pertinent parameters have a "exp($j\omega t$)" dependence. A consequence of this modification is that the diffusion length and the lifetime become time-varying functions, defined by[24]

$$L_n = \frac{L_{no}}{\sqrt{1 + j\omega t}};\ \tau = \frac{\tau_o}{1 + j\omega t} \tag{21}$$

with L_{no} and τ_o the dc values. The recombination and generation lifetimes become $\tau_r = \tau_{ro}/(1+j\omega\tau_{ro})$ and $\tau_g = \tau_{go}/(1+j\omega\tau_{go})$.

To determine the frequency-dependent nature of the equivalent circuit, we consider the impedance Z of the circuit in Fig. 10. It is given by

$$Z = \frac{1}{G_{tot} + j\omega C_{scr}} \tag{22}$$

where

$$G_{tot} = G_s + G_{r,scr} + G_{r,qnr} + G_{g,scr} + G_{g,qnr};\ C_{scr} = K_s \varepsilon_o / W \tag{23}$$

With $G_{r,scr}$ dominating over the relevant temperature range for sufficiently low surface recombination, Eq. (23) becomes

$$G_{tot} \approx G_{r,scr} = \frac{q^2 n_i W}{\tau_{scr} kT} \tag{24}$$

with $\tau_{scr} = \tau_{scro}/(1+j\omega\tau_{scro})$. The impedance now becomes

$$Z \approx \frac{G_{r,scr}^{-1}}{1 + j\omega C_{scr}/G_{r,scr}} = \frac{kT\tau_{scro}}{q^2 n_i W(1 + j\omega/\omega_c)} \tag{25}$$

with the corner-frequency, ω_c, given by

$$\omega_c = \frac{G_{r,scr}}{C_{scr}} = \frac{q^2 n_i W^2}{kTK_s \varepsilon_o \tau_{scro}} \tag{26}$$

The corner frequency depends on the scr recombination lifetime, τ_{scro}, the scr capacitance, C_{scr}, and $kT/(q^2 n_i W)$. Its temperature dependence is mainly due to n_i.

With the surface separated from the voltage probe, the photocurrent can only flow internally in the sample. The electrode measures the barrier lowering, which is the surface photovoltage V_{SPV} shown in Fig. 9. For light with high absorption coefficient, as applies for our experimental conditions, the photocurrent is mainly due to generation in the space-charge region

$$J_{ph} \approx J_{scr} = q\Phi(1-R)(1-\exp(-\alpha W)) \tag{27}$$

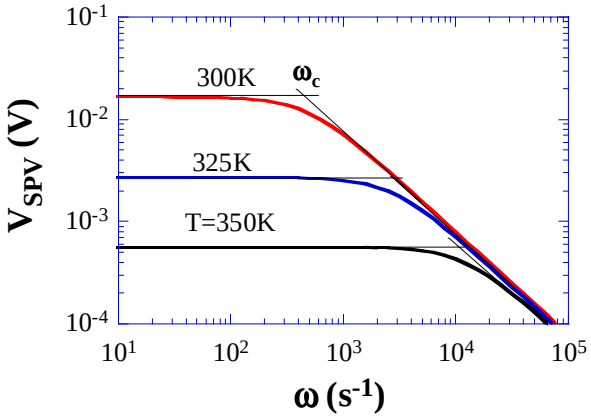

Fig. 11 V_{SPV} versus ω as a function of temperature for $\Phi = 10^{12}$ $cm^{-2}s^{-1}$, $R = 0.3$, $\alpha = 2x10^4$ cm^{-1}, $W = 0.8$ μm, $\tau_{scro} = 10^{-6}$ s, $\tau_{ro} = 10^{-5}$ s, $\tau_{go} = 10^{-3}$ s, $s_{ro} = 1000$ cm/s, $N_{A,epi} = 10^{15}$ cm^{-3}.

The current density depends on the photon flux density Φ, the reflectivity R, the absorption coefficient α, and the scr width W. The surface photovoltage is

$$V_{SPV} = J_{ph} Z \tag{28}$$

The surface voltage is plotted in Fig. 11 versus radial frequency as a function of temperature. The surface photovoltage obviously depends on the various lifetimes. The key question is: which lifetime has the major effect? To answer that question, we have calculated the effects of the various lifetimes. Varying the qnr lifetime τ_{qnro} from 10^{-6} to 10^{-3} s has almost no effect. The influence of the generation lifetime τ_{go} is only observed for τ_{scro} = 10^{-4}-10^{-3} s. Since τ_{go} is usually higher than τ_{scro}, it is obvious that τ_{go} also has minimal effect on V_{SPV}. Varying s_r from 10^2 to 10^7 cm/s has a significant effect on the curves. *Space-charge region recombination* is the dominant mechanism for low s_{ro} with τ_{scro} related to the corner frequency through the expression

$$\tau_{scro} = \frac{q^2 n_i W^2}{\omega_c kTK_s \varepsilon_o} = \frac{5.97x10^{-6} n_i W^2}{\omega_c (T/300)} \tag{29}$$

Experimental Results

We have characterized epitaxial wafers with two different doping profiles. The p/p^+ sample consists of an epitaxial layer, doped to 10^{15} cm^{-3}, deposited on a highly doped substrate, doped to 10^{18} cm^{-3}. The p/p^- sample consists of an epitaxial layer, doped to 10^{15}cm^{-3}, deposited on a moderately doped substrate, doped to 10^{15} cm^{-3}. The epitaxial layer thicknesses, t_{epi}, are 5 μm and 10 μm for both samples. The frequency and temperature dependence of the surface photovoltage of the 10 μm, p/p$^+$ sample are shown in Fig. 12. The agreement between theory and experiment is excellent. The lifetime τ_{scro} had to be changed from 0.95x10^{-6} s at 300K to 1.35x10^{-6} s at 330 K for theory and experiment to agree, consistent with lifetime increasing with increasing temperature in silicon.

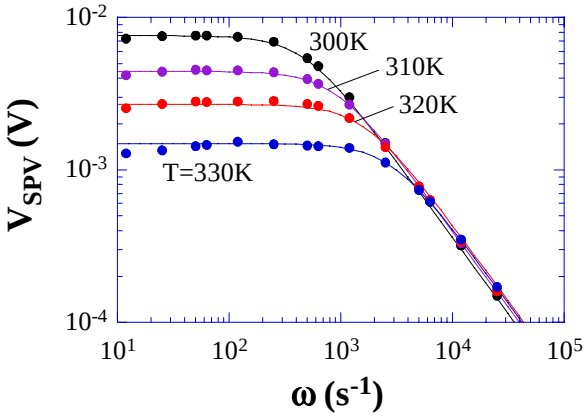

Fig. 12 Surface photovoltage versus frequency as a function of temperature. Experiment: t_{epi} = 10 μm, $N_{A,epi}$ = 10^{15} cm^{-3}, $N_{A,sub}$ = 10^{18} cm^{-3}. Theory: α = 2x10^4 cm^{-1}, W = 0.8 μm, τ_{ro} = 10^{-5} s, τ_{go} = 10^{-3} s, s_{ro} = 1000 cm/s, $N_{A,epi}$ = 10^{15} cm^{-3}.

The effects of substrate doping density and epi layer thickness are shown in Fig. 13. The agreement between experimental data and our theory is again excellent in all cases. The lifetimes of the p/p^+ samples are very similar to those for the p/p^- samples for both thicknesses. To compare the corona charge method with conventional surface photovoltage diffusion length measurements, we measured the diffusion length of both epitaxial wafers (p/p^+: $10^{15}/10^{18}$ cm^{-3}; p/p^+: $10^{15}/10^{15}$ cm^{-3}). In these measurements, photons with low absorption coefficients are used leading to carrier excitation through the epitaxial layer and a significant portion of the substrate. It has been shown that in that case, it is mainly the thickness of the epitaxial layer that is measured, if the diffusion length of the substrate is significantly lower than that of the pi layer, as it would be for the p/p^+ samples.[25]

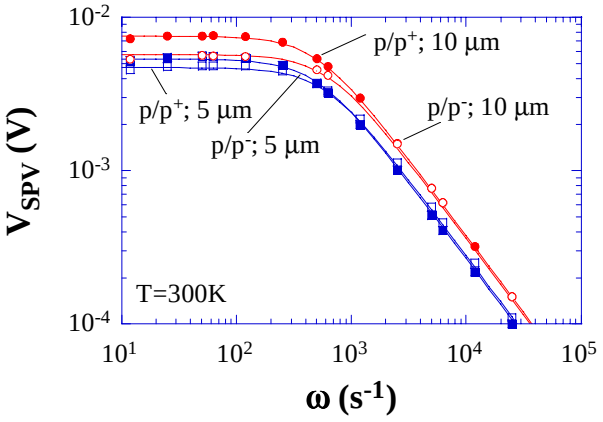

Fig. 13 Surface photovoltage versus frequency. τ_{scro}(p/p^+, 5 μm) = 0.8 μs, τ_{scro}(p/p^+, 10 μm) = 0.95 μs, τ_{scro}(p/p^-, 5 μm) = 0.95 μs, τ_{scro}(p/p^-, 10 μm) = 0.75 μs, τ_{go} = 1 ms, τ_{ro} = 10 μs, s_r = 1000 cm/s.

For the p/p^+ samples we find this to be the case. The diffusion lengths are 4.5 μm for the 5 μm thick layer and 7 μm for the 10 μm layer. For the p/p^- samples the diffusion lengths are 330 μm for the 5 μm thick layer and 304 μm for the 10 μm layer. As expected, here we find no relationship between diffusion length and epi layer thickness.

Conclusions

Epitaxial layers are difficult to characterize by conventional recombination lifetime or diffusion length measurements. Nevertheless, for sufficiently low surface/interface recombination velocities, it is possible to observe epi layer lifetime variations by measuring the effective lifetime, even though true lifetimes are difficult to extract because surface recombination velocities are generally unknown. The injection level dependence of the recombination lifetime can be used as an additional parameter in lifetime interpretation. It can lead to impurity identification by observing how the lifetime depends on injection level and whether the lifetime increases or decreases with injection. Temperature is an additional variant that is useful for activation energy extraction.

We have developed a theory to interpret *MOS capacitance* and *conductance* data measured versus frequency. One of the most important results of this work is that the frequency-dependent behavior at room temperature is governed by quasi-neutral region generation. This is surprising, because room temperature pulsed MOS capacitor and diode leakage current measurements, frequently used for lifetime determination, are governed by space-charge region generation with the generation lifetime localized to the space-charge region. One application of these measurements is the characterization of thin layers (epitaxial layers, denuded zones, or silicon-on-insulator). However, if quasi-neutral region generation dominates, then it is the minority carrier diffusion lengths that determines the characterization depth, not the space-charge region. But the diffusion length, being much longer than the layer thickness, is a poor parameter to use in such cases.

We have also developed the theory for optical *ac surface photovoltage* measurements and verified it with experimental data. We show that when the optically generated carriers are confined to the surface charge-induced space-charge region by using high absorption coefficient photons, the ac surface photovoltage response is governed by recombination in the space-charge region and is likely influenced by the surface. Recombination at the surface and in the quasi-neutral region plays a minor role, as do scr and qnr generation. Conventional surface photovoltage measurements gave minority carrier diffusion lengths of about the epi-layer thickness for the p/p^+ samples and about 300 μm for the p/p^- samples. Assuming the recombination lifetime or the diffusion length of the epi layer to be much higher than those of the heavily-doped substrate, one should not expect any values that are representative of the recombination properties of the epi layer since carrier generation during conventional SPV or during PCD measurements extends from the epi layer into the substrate. Only space-charge region confined measurements yield information about the epitaxial film. Such measurements are most commonly made through reverse-biased measurements of pn junctions or field-induced junctions. The frequency-dependent method discussed here, adds an additional option to such measurement. It is attractive because it is contactless using optical excitation.

Acknowledgments

The research leading to this paper was partially funded by the Silicon Wafer Engineering and Defect Science Consortium (SiWEDS) (Intel, Komatsu Electronic Metals, MEMC Electronic Materials, Mitsubishi Silicon, Nippon Steel, Okmetic, Sumitomo Sitix Silicon, Texas Instruments and Wacker Siltronic Corp.).

References

[1] J. R. Haynes and W. Shockley, "The Mobility and Life of Injected Holes and Electrons in Germanium," *Phys. Rev*. **81**, 835-843, March 1951.

[2] K. Graff and H. Pieper, "The Properties of Iron in Silicon," *J. Electrochem. Soc*. **128**, 669-674, March 1981; L. C. Kimerling and J .L. Benton, "Electronically Controlled Reactions of Interstitial Iron in Silicon," *Physica* **116B**, 297-300, Feb. 1983.

[3] G. Zoth and W. Bergholz, "A Fast, Preparation-Free Method to Detect Iron in Silicon," *J. Appl. Phys*. **67**, 6764-6771, June 1990.

[4] D. K. Schroder, *Semiconductor Material and Device Characterization*, Second Ed., Wiley-Interscience, New York, 1998.

[5] C. Swiatkowski , "Lifetime Measured by Low Injection Level μ-PCD Technique," in *Recombination Lifetime Measurements in Silicon* (D.C. Gupta, F.R. Bacher, and W.M. Hughes, eds), ASTM **STP 1340**, 80-87, 1998.

[6] T. Pavelka and Z. Batari, "Lifetime Measurements in SOI and Epi Structures," in *Analytical and Diagnostic Techniques for Semiconductor Materials, Devices, and Processes* (B. O. Kolbesen, C. Claeys, P. Stallhofer, F. Tardiff, J. Benton, T. Shaffner, D. Schroder, S. Kishino, and P. Rai-Choudhury, eds.), Electrochem. Soc. **ECS PV 99-16**, 48-55, 1999.

[7] C. Claeys, E. Simoen, A. Poyai, and A. Czerwinski, "Electrical Quality Assessment of Epitaxial Wafers Based on p-n Junction Diagnostics," *J. Electrochem. Soc*. **146**, 3429-3434, Sept. 1999.

[8] S. Y. Lee and D. K. Schroder, "Thin p/p^+ Epitaxial Layer Characterization With the Pulsed MOS Capacitor," *Solid State Electron.* **43**, 103-111, Jan. 1999.

[9] D. K. Schroder, J. E. Park, S. E. Tan, B. D. Choi, S. Kishino, H. Yoshida, "Frequency Domain Lifetime Characterization," *IEEE Trans. Electron Dev*., accepted for publication.

[10] D. K. Schroder, M. S. Fung, R. L. Verkuil, S. Pandey, W. H. Howland, and M. Kleefstra, "Corona-Oxide-Semiconductor Generation Lifetime Characterization," *Solid-State Electr*. **42**, 505-512, April 1998.

[11] Y. Murakami, H. Abe, and T. Shingyouji, "Calculation of Diffusion Component of Leakage Current in pn Junctions Formed in Various Types of Silicon Wafers,", *Japan. J. Appl. Phys*. **34**, 1477-1482, March 1995.

[12] D. K. Schroder, "Carrier Lifetimes in Silicon," *IEEE Trans. Electron Dev*. **44**, 160-170, Jan. 1997.

[13] P. Eichinger, "New Developments of the ELYMAT Technique," in *Recombination Lifetime Measurements in Silicon* (D. C. Gupta, F. R. Bacher, and W. M. Hughes, eds), ASTM **STP 1340**, 101-111, 1998.

[14] H. Hashizume, S. Sumie, and Y. Nakai, "Carrier Lifetime Measurements by Microwave Photoconductivity Decay Method," in *Recombination Lifetime Measurements in Silicon* (D.C. Gupta, F.R. Bacher, and W.M. Hughes, eds), ASTM **STP 1340**, 47-58, 1998.

[15] E. O. Johnson, "Large-Signal Surface Photovoltage Studies With Germanium, " *Phys. Rev.* **111**, 153-166, July 1958; A. M. Hoff, T. C. Esry, and K. Nauka, "Monitoring Plasma Damage: A Real-Time, Noncontact Approach," *Solid State Technol*. **39**, 139-152, July 1996.

[16] K. Lehovec and A. Slobodskoy, "Impedance of Semiconductor-Insulator-Metal Capacitors," *Solid-State Electron*. **7**, 59-79, Jan. 1964.

[17] S. R. Hofstein and G. Warfield, "Physical Limitations on the Frequency Response of a Semiconductor Surface Inversion Layer," *Solid-State Electron*. **8**, 321-341, March 1965.

[18] E.H. Nicollian and J.R. Brews, *MOS Physics and Technology*, Wiley, New York, 1982.

[19] G. Baccarani, C. A. Baffoni, M. Rudan, and G. Spadini, "Majority- and Minority-Carrier Lifetime in MOS Structures," *Solid-State Electron*. **18**, 1115-1122, Dec. 1975.
[20] J. E. Park, D. K. Schroder, S. E. Tan, B. D. Choi, M. Fletcher, A. Buczkowski, and F. Kirscht, "Epitaxial Layer Lifetime Characterization in the Frequency Domain," this volume.
[21] Lord Kelvin, "On a Method of Measuring Contact Electricity," Nature, April 1881; "Contact Electricity of Metals," *Phil. Mag*. **46**, 82-121, 1898.
[22] L. Kronik and Y. Shapira, "Surface Photovoltage Phenomena: Theory, Experiment, and Applications", *Surf. Sci. Rep*. **37**, 1-206, Dec. 1999.
[23] Semiconductor Diagnostics, Inc. Manual "Contamination Monitoring System Based on SPV Diffusion Length Measurements," SDI, 1993.
[24] J. P. McKelvey, *Solid State and Semiconductor Physics*, Harper and Row, New York, 1966.
[25] J. W. Slotboom and M. J. J. Theunissen, "Impact of Silicon Substrates on Leakage Current," *IEEE Electron Dev. Lett*. **EDL-4**, 403-406, Nov. 1983; D.K. Schroder, "Effective Lifetimes in High Quality Silicon Devices," *Solid State Electron*. **27**, 247-251, March 1984; C. W. Pearce and R. J. Jaccodine, "An Analytical Model of Diffusion Current in Intrinsically Gettered Structures Based on Intentional Experiments," *IEEE Trans. Electron Dev*. **38**, 2155-2160, Sept. 1991.